Temperature dependence of photoluminescence in modulation-doped pseudomorphic high electron mobility transistor $Al_xGa_{1-x}As/In_yGa_{1-y}As/GaAs$ structures

P. W. Yu and B. Jogai
University Research Center, Wright State University, Dayton, Ohio 45435

T. J. Rogers, P. A. Martin, and J. M. Ballingall
Martin Marietta Laboratories Syracuse, Syracuse, New York 13221

(Received 31 May 1994; accepted for publication 22 August 1994)

We report the temperature-dependent characteristics of photoluminescence emission in modulation δ-doped $Al_xGa_{1-x}As/In_yGa_{1-y}As/GaAs$ structures. Transition energies are analyzed using a self-consistent solution of the coupled $\mathbf{k}\cdot\mathbf{P}$ Hamiltonian–Poisson equation. At low temperatures, dominant emissions are due to the transitions from the first electron subband to the first heavy-hole subband and from the second electron subband to the first heavy-hole subband irrespective of the location of modulation doping. The second hole subband related transitions associated with the first electron subband or the second electron subband emerges with increasing temperature depending on the location of doping. The relative intensities of the transitions from the first and second electron subbands to the first heavy-hole subband transitions are analyzed as a function of the Fermi energy position. An excellent agreement is found between the measurements and calculations. © *1994 American Institute of Physics.*

I. INTRODUCTION

The pseudomorphically strained InGaAs layer has been demonstrated[1] to be an excellent channel layer for the modulation-doped $Al_xGa_{1-x}As/In_yGa_{1-y}As/GaAs$ pseudomorphic high electron mobility transistor (p-HEMT). The use of an InGaAs channel layer results in a larger conduction-band discontinuity. It is possible to use $Al_xGa_{1-x}As$ ($x \leqslant 0.2$), in which no DX centers are present, without sacrificing from two-dimensional electron gas (2DEG) carrier density. Such a p-HEMT structure has emerged as the device of choice for power microwave devices in the 30–100 GHz range and for many high-speed digital applications.[2,3] Electrons are confined at the heterojunction not only by their electrostatic attraction to ionized impurities in the large gap $Al_xGa_{1-x}As$ layer, but also by the presence of an $In_yGa_{1-y}As$ quantum well (QW) between the $Al_xGa_{1-x}As$ and GaAs. This quantum well also confines photogenerated holes, which makes photoluminescence (PL) a useful tool for studying the 2DEG in these technologically important structures. The thin $In_yGa_{1-y}As$ layer, with its lattice constant larger than GaAs is under biaxial compression to force a lattice match to GaAs substrates. The strain (in the range of 1%–2%) separates the light- and heavy-hole states and shifts the band gap to higher energy. Much of the previous work[4–6] involving PL from modulation-doped $Al_xGa_{1-x}As/In_yGa_{1-y}As/GaAs$ p-HEMT structures were centered on the correlation between the sheet carrier concentration and PL line width. Electric field effects on low-temperature PL line shape and energy were studied[7] by modulating the Fermi level with a reverse gate voltage. The excitonic resonant enhancement of the Fermi-edge singularity was observed[8] from a system under a near-resonant condition between an exciton level from a higher electron subband and the Fermi level. However, detailed study on the origin of transitions has not been made.

In the present work, we studied temperature-dependent PL characteristics for p-HEMT $Al_xGa_{1-x}As/In_yGa_{1-y}As/GaAs$ n-type modulation-doped structures. The doping was made at single side or double sides of the $In_yGa_{1-y}As$ QW. The transition energies were analyzed based on calculations made using a self-consistent solution[9] of the coupled $\mathbf{k}\cdot\mathbf{p}$ Hamiltonian–Poisson equation which gives the effective band gap, the Fermi energy, electron- and hole-subband energies, and sheet carrier concentration. We find that the type of PL transition depends on the location of doping. The PL intensity was analyzed considering the subband filling and the overlapping factor coming from the band-bending behavior.

II. EXPERIMENTAL DETAILS

Ten p-HEMT wafers, with typical structures shown in Figs. 1(a) and 1(b) and individual structure parameters given in Table I, were used in this study. They consist of two types of structures: namely, doping made at double sides or single side of the $In_yGa_{1-y}As$ QW as shown in Figs. 1(a) and 1(b), respectively. The structures doped at double sides consist of Si δ doping, $Al_xGa_{1-x}As$ spacer layer, $In_yGa_{1-y}As$ QW, undoped 50 Å $Al_xGa_{1-x}As$ layer, and a 50 Å $Al_xGa_{1-x}As$ layer doped with a Si 9×10^{17} cm^{-2}. The Si δ dopings were 3×, 4×, and 5×10^{12} cm^{-2}. The spacer layer width varied from 25 to 180 Å so that the number of electrons which transferred from the δ layer to the $In_yGa_{1-y}As$ also varied. The double-side Si doping above and below the QW well contrasts with a single-side Si doping only above the well in terms of producing different types of transitions. Sample J was grown by organometallic vapor phase epitaxy (OMVPE) at Kopin Corporation and other samples were grown in Varian Gen-II molecular beam epitaxy (MBE) apparatus using solid source As, with $[As_4]/[Ga]$ beam equivalent pressure ratio of ~15.

 0021-8979/94/76(11)/7535/6/$6.00

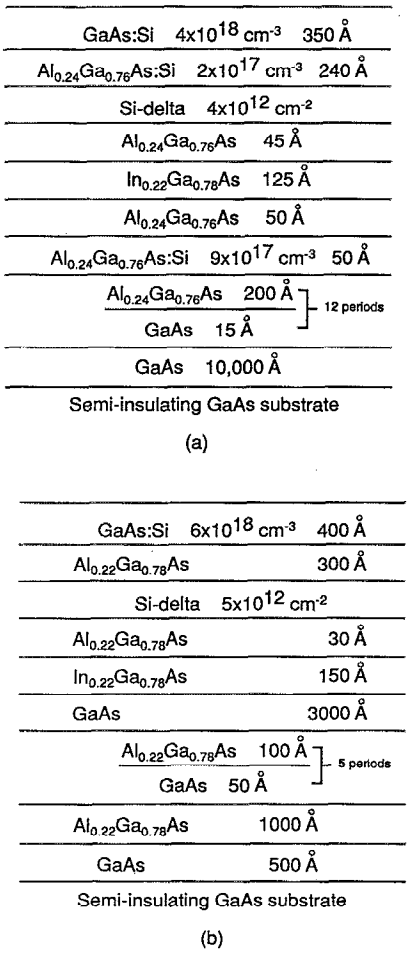

FIG. 1. (a) Nominal structure of the p-HEMT A. There are double Si dopings above and below the InGaAs QW. (b) Nominal structure of the p-HEMT H. There is single Si doping above the InGaAs QW.

PL measurements were made using a variable temperature Janis optical dewar. The 5145 Å line of an Ar ion laser was used as an excitation source with density of 10^{-3}–10^{1} W/cm^2. PL spectra were obtained with a Spex monochromator of focal length $f=0.5$ m and were detected with a liquid-nitrogen-cooled North-Coast optics Ge detector. A standard synchronous technique was used with a lock-in amplifier.

TABLE I. Samples used and their structure parameters.

No.	Doping	General description	Well width (Å)	Spacer layer (Å)	Si delta doping (cm^{-2})
A	Double	Fig. 1(a)	125	45	4×10^{12}
B	Double	Fig. 1(a)	125	25	4×10^{12}
C	Double	Fig. 1(a)	125	90	4×10^{12}
D	Double	Fig. 1(a)	125	180	4×10^{12}
E	Double	Fig. 1(a)	125	45	0
F	Double	Fig. 1(a)	125	45	3×10^{12}
G	Double	Fig. 1(a)	125	45	5×10^{12}
H	Single	Fig. 1(b)	150	30	5×10^{12}
I	Single	Fig. 1(b)	100	45	5×10^{12}
J	Single	Fig. 1(b)	150	60	5×10^{12}

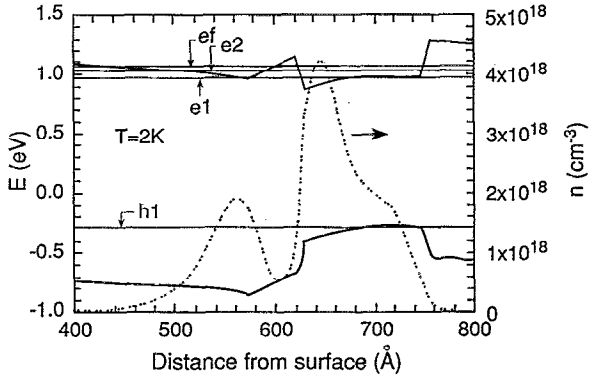

FIG. 2. $T=2$ K calculated band structure (solid lines), carrier concentration (dotted line), and Fermi energy ef, the first conduction subband $e1$, second conduction subband $e2$, and the first heavy-hole valence subband $h1$.

III. CALCULATION

We previously described a quantum-mechanical calculation[9] of the band edges and electron distribution of δ-doped $Al_xGa_{1-x}As/In_yGa_{1-y}As/GaAs$ p-HEMT structure. The theory was accomplished with a four-band $\mathbf{k}\cdot\mathbf{P}$ calculation of the band structure, coupled self-consistently with a solution of the Poisson equation. The eigenstates were described in terms of a basis consisting of electron, heavy-hole, light-hole, and split-off bulk states. The exchange-correlation potential was calculated from density functional theory within the local-density approximation.

Recently, this work was extended to include strain-induced band mixing and strain-induced corrections to the spin-orbit interaction.[10] Surface donor and acceptor states were included to pin the Fermi level at $E_c-0.75$ eV, which is known to occur for a free surface of GaAs. The model can also incorporate interface states at inverted GaAs/AlGaAs and other interfaces. The density of these states is uncertain depending on the growth conditions. In the present calculations, interface states were omitted. The binary material parameters used to calculate the band structure are also given in Ref. 9. We analyzed experimental data obtained at $T=2$, 77, and 300 K even though the measurements were made at $T=2$–300 K. The values for the band gap of $In_yGa_{1-y}As$ are as follows:[11–13]

$$E_g(y)=1.519-1.584y+0.475y^2(\text{eV}) \quad \text{at } T=2 \text{ K}, \tag{1}$$

$$E_g(y)=1.508-1.580y+0.496y^2(\text{eV}) \quad \text{at } T=77 \text{ K}, \tag{2}$$

$$E_g(y)=1.423-1.500y+0.436y^2(\text{eV}) \quad \text{at } T=300 \text{ K}. \tag{3}$$

The temperature-dependent values of the band gaps of $Al_xGa_{1-x}As$ were obtained[14] from the Varshni-type relation. The calculated band edges, electron concentration profiles, the first and second electron subbands $e1$ and $e2$, the first heavy-hole subband $h1$, and the Fermi energy ef at $T=2$ K are shown in Fig. 2 for the region around the QW for sample A, which is double side doped.

Even though double-sided Si doping was used, a heavier doping above the QW gives a strong band bending at the

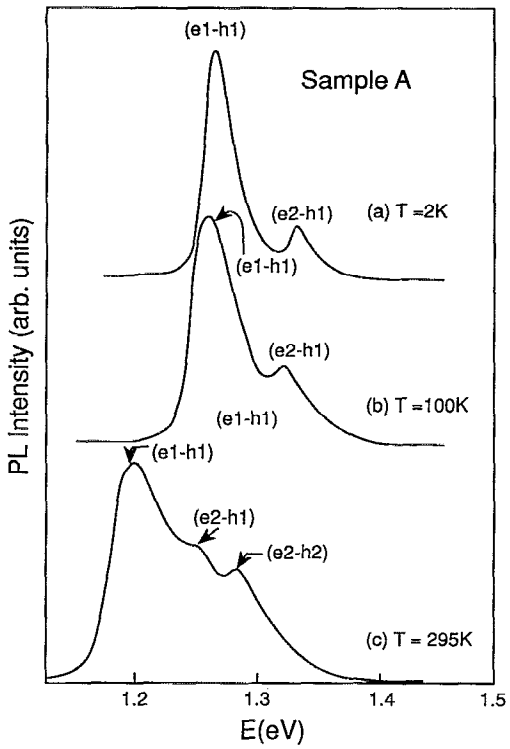

FIG. 3. PL spectra of sample A at T=2, 100, and 295 K.

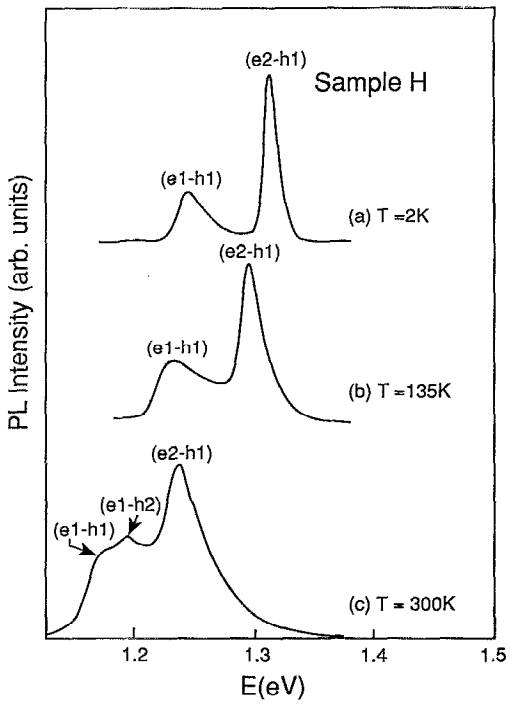

FIG. 4. PL spectra of sample H at T=2, 135, and 300 K.

spacer layer and the region near the spacer layer in the QW and almost flat-band profile in the region away from the spacer layer.

IV. RESULTS AND DISCUSSION

Figures (3) and (4) show PL spectra at different temperatures for samples A and H, which have sample structures shown in Figs. 1(a) and 1(b), respectively. Sample A is doped with Si on both sides of the $In_{0.22}Ga_{0.78}As$ QW, whereas sample H is δ doped only one side above the $In_{0.22}Ga_{0.78}As$ QW. At low-temperatures dominant PL emissions are from the transitions between the $e1$ and $h1$ subbands and between the $e2$ and $h1$ subbands, respectively, designated as ($e1$-$h1$) and ($e2$-$h1$) irrespective of the location for doping. However, as the temperature increases, a doping location-dependent transition appears: transitions ($e2$-$h2$) and ($e1$-$h2$) emerge, respectively, from samples A and H at high temperatures. Figure 5 and 6 show the detailed relation between the transition energy and temperature for samples A and H. PL measurements for all other structures basically show the same PL characteristics as shown for samples A and H: (1) dominant transitions at low temperatures are due to the ($e1$-$h1$) and ($e2$-$h1$), (2) the increase of temperature brings an additional transition ($e2$-$h2$) or ($e1$-$h2$), and (3) the ($e2$-$h2$) and ($e1$-$h2$) transitions originate, respectively, from the double- and single-side doped samples. It can be explained easily in terms of band bending, that parity allowed transition ($e2$-$h2$) for the structure doped at double sides and nonparity allowed transition ($e1$-$h2$) for the structure doped at single side are preferred, since the band bending yields a triangular and somewhat flat potential and mainly a triangular potential, respectively, for the double-and single-side doped structures. We will, now, discuss the availability of holes at the $h2$ subband.

Figure 7 shows the relationship between the integrated emission intensity and 10^3/T of the transitions ($e1$-$h1$) and

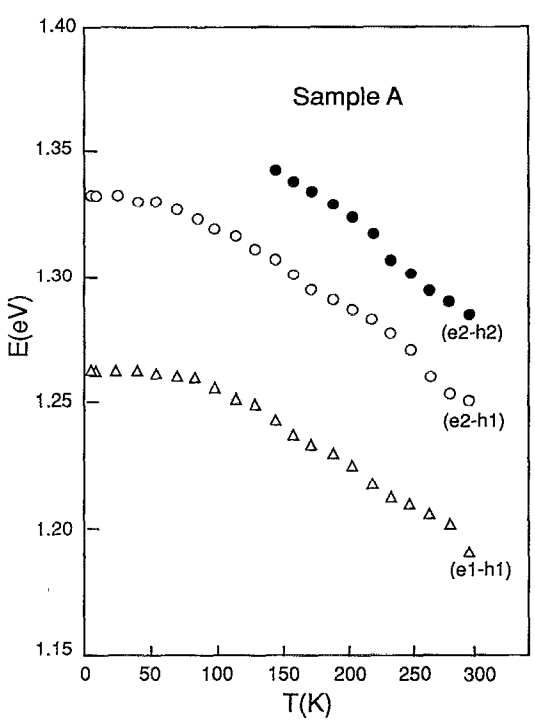

FIG. 5. Temperature dependence of the energies of the transition ($e1$-$h1$), ($e2$-$h1$), and ($e2$-$h2$) for sample A.

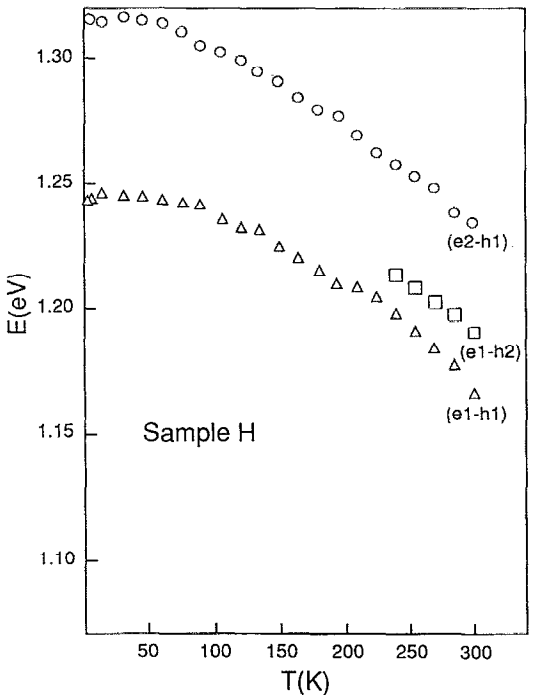

FIG. 6. Temperature dependence of the energies of the transition ($e1$-$h1$), ($e1$-$h2$), and ($e2$-$h1$) for sample H.

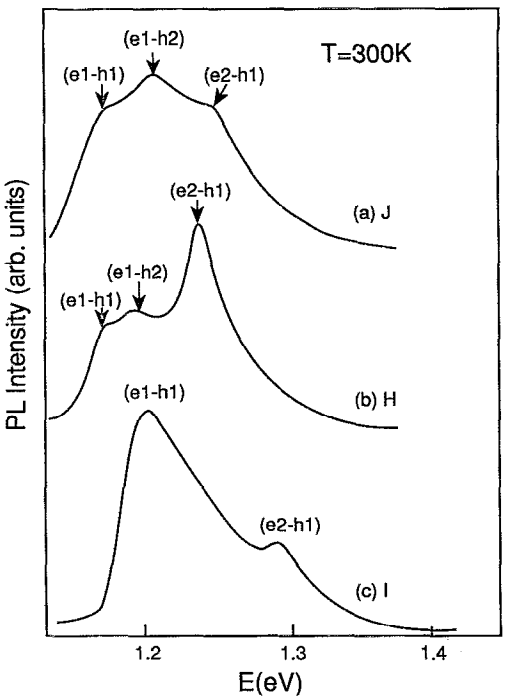

FIG. 8. Different PL spectra obtained from samples J, H, and I at $T=300$ K.

($e2$-$h1$) for sample G. The solid lines are fit calculated with the following equation:

$$I=C_1/[1+C_2\exp(-E_a/kT)], \tag{4}$$

where I is the integrated emission intensity, E_a is an activation energy, and C_1 and C_2 are constants. From the fit, E_a of 30 ± 2 and 29 ± 2 meV, respectively, from the ($e1$-$h1$) and ($e2$-$h1$) transitions is obtained. These values are consistent with the calculated value of 30.2 meV, the difference between the $h1$ and $h2$ subband energies designated as ($h2$-$h1$). We attribute the population of holes at the $h2$ subband to the thermal excitation from the $h1$ subband with increasing temperature. Another evidence of the thermal excitation is present in Fig. 8. The figure shows three PL spectra at $T=300$ K from single-side-doped structures J, H, and I. The three spectra show different characteristics in terms of the dominance of peak intensity between the transitions of the ($e1$-$h1$) and ($e1$-$h2$) emissions: Sample J shows the dominance of the ($e1$-$h2$) transition over the ($e1$-$h1$), sample H shows almost comparable strength between the two, and sample I shows only ($e1$-$h1$) transition. These characteristics originate from the difference of ($h1$-$h2$). The calculated values of ($h1$-$h2$) are respectively, 26, 36, and 53 meV for structure J, H, and I. The degree of the hole thermal excitation depends on the value of ($h1$-$h2$). This is exactly illustrated in Fig. 8. However, the three samples show the usual ($e1$-$h1$) and ($e2$-$h1$) transitions at low temperatures as shown in Fig. 4. So, the near-room-temperature PL characteristics strongly depend on the location of doping and the value of ($h1$-$h2$). Other evidence of the hole thermal excitation can be found from Figs. 5 and 6. The ($e2$-$h2$) and ($e1$-$h2$) transitions begin to appear approximately at 140 and 240 K. This is well correlated with the values of 27 and 37 meV for ($h1$-$h2$) for structure A and the H in Figs. 5 and 6.

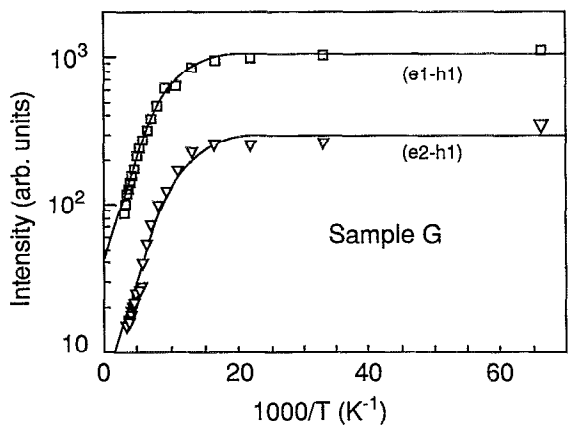

FIG. 7. Temperature dependence of the integrated intensities of the transitions ($e1$-$h1$) and ($e2$-$h1$) for sample G. The solid lines are fit to Eq. (3).

Now we turn our attention to the $T=2$ K relative strength of ($e1$-$h1$) and ($e2$-$h1$) transitions from the same structures shown in Fig. 1(a) except for the spacer layer width and doping level. Figure 9 shows PL spectra from structures B, A, and C.

All three samples are double-side doped. The only difference among the structures is the spacer-layer width, which changes the number of electrons transferring to the InGaAs QW from the δ-doped region. The strength of the ($e2$-$h1$) transition relative to that of the ($e1$-$h1$) transition clearly decreases with increasing spacer-layer thickness. In order to understand this observation, the relative integrated emission

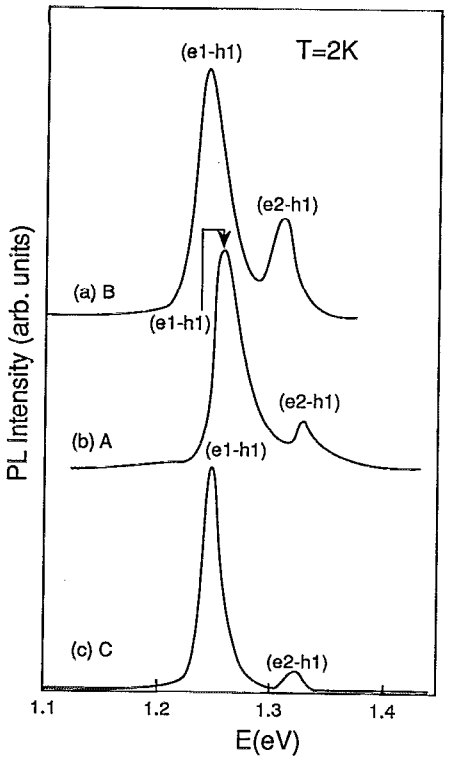

FIG. 9. T=2 K Pl spectra obtained from samples B, A, and C. Note the variation of intensity of the ($e2$-$h1$) transition relative to that of the ($e1$-$h1$) transition.

intensity of the ($e2$-$h1$) and ($e1$-$h1$) transitions(I_{21}/I_{11}) is plotted with the energy difference of the Fermi and the $e2$ subband energies (ef-$e2=\Delta E_{f2}$) for six samples in Fig. 10. The solid line is based on a calculation of the square of the i to j subband optical matrix element of the involved transitions. Recently, Lyo and Jones[15] developed a theory describing the PL line shape in modulation-doped n-type material. According to the model a PL emission rate is obtained by multiplying the square of the i to j band transition matrix element by the line-shape function $F_{ij}/\hbar$. The line-shape function F_{ij} is defined by

$$F_{ij}(\omega)=A\,\theta(\omega)\int_0^{\omega} d\zeta f(\zeta-\mu_{vj})f(\omega-\zeta-\mu_{ci})L(\omega,\zeta), \tag{5}$$

where ω is the photon energy minus the effective band gap, μ_{ci} and μ_{vj} are ith band electron and jth band hole chemical potential, $f(x)$ are the Fermi function, A is a normalization parameter, $\theta(\omega)$ is the unit step function. The Lorentzian factor L accounts for the processes associated with direct transition in $\mathbf{k}$ space and indirect transition assisted by impurities. When we designated the square of the initial i to final j state transition matrix as O_{ij}, O_{ij} can be written[16] as

$$O_{ij}=|\hat{e}\cdot\mathbf{P}_{ij}|^2, \tag{6}$$

where $\hat{e}$ is the unit vector potential and $P_{ij}=-i\hbar\int\phi_j\nabla_r\phi_i dr$. ϕ_i and ϕ_j are the initial i state and final j state wave function. So, the PL intensity from the i state to the j state, I_{ij}, is given by $1/\hbar$, O_{ij}, F_{ij}. Under the conditions of low temperature and low excitation, the available range for hole $\mathbf{k}$ vector $\mathbf{k}^h$, is limited by the degree of hole localization due to potential fluctuation in a nonideal real crystal. Then $k_F^h \ll k_F^e$, where k_F^i is the Fermi wave vector for i particle and F_{11} and F_{12} become constants. So, I_{21}/I_{11} is proportional to O_{21}/O_{11}. The solid line in Fig. 10 is the plot of O_{21}/O_{11} values, which are calculated[10] using a self-consistent solution of the coupled $\mathbf{k}\cdot\mathbf{P}$ Hamiltonian–Poisson equation. As sheet carrier concentration in the well decreases, the band bending decreases. Then, the QW shape becomes flat and the overlap between the $e1$ and $h1$ wave functions increases whereas the overlap between the $e1$ and $h2$ wave functions decreases. When $ef>e2$ with the increase of sheet carrier concentration, the band bending becomes sharper. Then, the overlap between the $e1$ and $h1$ wave functions decreases and the overlap between the $e2$ and $h1$ wave functions increases.

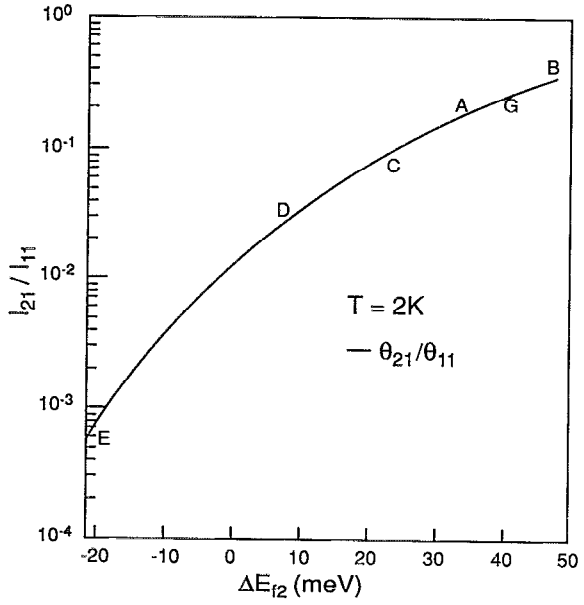

FIG. 10. Ratio of integrated PL intensity of $e2$-$h1$ transition to that of $e1$-$h1$ transition vs ΔE_{F2} relation ($\Delta E_{F2}=ef-e2$).

V. CONCLUSION

Temperature-dependent PL measurements were made for ten p-HEMT $Al_xGa_{1-x}As/In_yGa_{1-y}As/GaAs$ structures. The structures doped singly above the $In_yGa_{1-y}As$ well and doped doubly above and below the well were chosen. A theoretical calculation using a self-consistent solution of the coupled $\mathbf{k}\cdot\mathbf{P}$ Hamiltonian–Poisson equation was used to obtain the band edge, the Fermi energy, electron- and hole-subband energies, and sheet carrier concentration. Two dominant emissions at low-temperatures are due to the ($e1$-$h1$) and ($e2$-$h1$) transitions regardless of the location of doping. However, with the increase of temperature, new emission of the ($e1$-$h2$) and ($e2$-$h2$) transitions appears, respectively, from the singly and doubly doped structures. The emergence of the ($e1$-$h2$) and ($e2$-$h2$) transitions can be attributed to the shape of band edges in the structures, respectively doped

singly and doubly, which selectivity boost the overlap between respective transitions. The availability of the hole at the $h2$ subband is due to the thermal excitation of hole from the $h1$ to $h2$ subband. Therefore, the energy difference between the $h1$ and $h2$ subbands affects the intensity of the new transition over the existing ($e1$-$h1$) and ($e2$-$h1$) transitions. Measurements taken only at room temperature can cause difficulty in identifying the type of emission. The thermal excitation from the $h1$ to the $h2$ subband can be demonstrated by using the relationship between emission intensity and temperature, room-temperature emission characteristics of the singly doped structures, and the emerging intensity of the new emission. At low temperatures, the relative strength of the ($e1$-$h1$) and ($e2$-$h1$) transitions can be explained by the square of the initial to final band transition matrix. This is clear in view of the greater band bending with increasing sheet carrier concentration in the InGaAs well, which causes the difference of overlapping of the respective electron and hole wave functions.

ACKNOWLEDGMENTS

The authors express their sincere gratitude to W. Rice for photoluminescence measurements, R. E. Sherriff and C. W. Litton for technical support, D. C. Streit and TRW for sample H and S. K. Shastry and his associates at Kopin for the OMVPE sample. The work of P. W. Y. and B. J. was performed at Wright Laboratories, Solid State Electronics Directorate (WL/EL), Wright Patterson Air Force Base under USAF Contract No. F33615-91-C-1765. J. M. B., P. A. M., and T. J. R. were supported by the Advanced Research Projects Agency (ARPA) under the MIMIC Program, Contract No. F33615-91-C-1784. Further ARPA support came through the ARPA Tri-Service Epitaxial Characterization Program.

[1] J. J. Rosenberg, M. Benlamri, P. D. Kirchner, J. M. Woodall, and G. L. Pettit, IEEE Electron. Device Lett. **EDL-6**, 491 (1985).
[2] J. M. Ballingall, P. A. Martin, J. Mazurowski, P. Ho, P. C. Chao, P. M. Smith, and K. H. G. Duh, Thin Solid Films **231**, 95 (1993).
[3] T. Mimura, in *Semiconductors and Semimetals,* edited by T. Ikoma (Academic, Boston, 1990), Vol. 30, p. 157.
[4] A. Dodabalapur, V. P. Kesan, D. R. Hinson, D. P. Neikirk, and B. G. Streetman, Appl. Phys. Lett. **54**, 1675 (1989).
[5] H. Brugger, H. Müssig, C. Wölk, K. Kern, and D. Heitmann, Appl. Phys. Lett. **59**, 2739 (1991).
[6] S. K. Brierley, J. Appl. Phys. **74**, 2766 (1993).
[7] J. M. Gilpérez, J. L. Sánchez-Rojas, E. Muñoz, E. Calleja, J. P. R. David, and G. Hill, Appl. Phys. Lett. **61**, 1225 (1992).
[8] W. Chen, M. Fritz, W. Walecki, A. V. Nurmikko, D. Ackley, J. M. Hong, and L. L. Chang, Phys. Rev. B **45**, 8464 (1992).
[9] B. Jogai, P. W. Yu, and D. C. Streit, J. Appl. Phys. **75**, 1586 (1994).
[10] B. Jogai, J. Appl. Phys. (1994) (to be published).
[11] K. H. Goetz, D. Bimberg, H. Jür, J. Seiders, A. V. Salomenov, G. F. Glinskii, M. Razeghi, and J. Robin, J. Appl. Phys. **54**, 4543 (1983).
[12] D. J. Arent, K. Deneffe, C. Van Hoof, J. De Broeck, and G. Borghs, J. Appl. Phys. **66**, 1739 (1989).
[13] L. Hřivnák, Phys. Status Solidi A **166**, K73 (1989).
[14] M. El Allai, C. B. Sørensen, E. Veje, and P. Tidemand-Petersson, Phys. Rev. B **48**, 4398 (1993).
[15] S. K. Lyo and E. D. Jones, Phys. Rev. B **38**, 4113 (1988).
[16] See, for example, F. Bassani and C. F. Parrasvacini, *Electronic States and Optical Properties in Solid* (Pergamon, New York, 1975).